EARTH SURFACE PROCESSES AND LANDFORMS
Earth Surf. Process. Landforms **34**, 1994–2007 (2009)

Published online 13 November 2009 in Wiley InterScience
(www.interscience.wiley.com) DOI: 10.1002/esp.1884

The implications of data selection for regional erosion and sediment yield modelling

Joris de Vente,[1,2]* Jean Poesen,[1] Gerard Govers[1] and Carolina Boix-Fayos[3]
[1] Physical and Regional Geography Research Group, Katholieke Universiteit Leuven GEO-INSTITUTE, Celestijnenlaan 200 E, 3001, Heverlee, Belgium
[2] Estación Experimental de Zonas Áridas (EEZA-CSIC), Desertification and Geoecology Department, General Segura 1, 04001, Almeria, Spain
[3] Centro de Edafología y Biología Aplicada del Segura (CEBAS-CSIC), Soil Erosion and Conservation Department, Campus Universitario de Espinardo, PO Box 164, 30100, Murcia, Spain

Received 14 October 2008; Revised 22 June 2009; Accepted 6 July 2009

*Correspondence to: J. de Vente, [2]Estación Experimental de Zonas Áridas (EEZA-CSIC), Desertification and Geoecology Department, General Segura 1, 04001, Almeria, Spain. Email: Joris@eeza.csic.es

ESPL
Earth Surface Processes and Landforms

ABSTRACT: Regional environmental models often require detailed data on topography, land cover, soil, and climate. Remote sensing derived data form an increasingly important source of information for these models. Yet, it is often not easy to decide what the most feasible source of information is and how different input data affect model outcomes. This paper compares the quality and performance of remote sensing derived data for regional soil erosion and sediment yield modelling with the WATEM-SEDEM model in south-east Spain. An ASTER-derived digital elevation model (DEM) was compared with the DEM obtained from the Shuttle Radar Topography Mission (SRTM), and land cover information from the CORINE database (CLC2000) was compared with classified ASTER satellite images. The SRTM DEM provided more accurate estimates of slope gradient and upslope drainage area than the ASTER DEM. The classified ASTER images provided a high accuracy (90%) land cover map, and due to its higher resolution, it showed a more fragmented landscape than the CORINE land cover data. Notwithstanding the differences in quality and level of detail, CORINE and ASTER land cover data in combination with the SRTM DEM or ASTER DEM allowed accurate predictions of sediment yield at the catchment scale. Although the absolute values of erosion and sediment deposition were different, the qualitative spatial pattern of the major sources and sinks of sediments was comparable, irrespective of the DEM and land cover data used. However, due to its lower accuracy, the quantitative spatial pattern of predictions with the ASTER DEM will be worse than with the SRTM DEM. Therefore, the SRTM DEM in combination with ASTER-derived land cover data presumably provide most accurate spatially distributed estimates of soil erosion and sediment yield. Nevertheless, model calibration is required for each data set and resolution and validation of the spatial pattern of predictions is urgently needed. Copyright © 2009 John Wiley & Sons, Ltd.

KEYWORDS: resolution; land cover; topography; SRTM; ASTER; CORINE; soil erosion

Introduction

Availability of good quality and sufficiently detailed input data is often one of the limiting factors for successful application of environmental models at a regional scale (Renschler and Harbor, 2002; Van Rompaey and Govers, 2002; Merritt *et al.*, 2003; de Vente and Poesen, 2005). Many model applications are therefore limited to relatively small study areas for which detailed and high-resolution information on environmental factors such as land cover, climate, topography and soils are available. However, to assist policymakers and environmental management agencies, models often need to be applicable to large drainage basins or even regionally or globally. Yet, commonly available data sets with a regional coverage often show little detail and are typically at a spatial resolution of 1 km or less. The same accounts for data-poor regions of the world, where, if any data are available, the spatial resolution is often very low. This lack of detail in representation of surface characteristics makes reliable application of many environmental models troublesome at the regional or even at the drainage basin scale. Renschler and Harbor (2002) also reported that the use of commonly available data instead of research-grade data can have an important impact on the outcome of soil erosion models, and therefore they recommended that models should be developed with realistic data availability in mind.

With the increasing availability of relatively high-resolution land cover and elevation data with a global coverage from remote sensing sources, the problem of data availability appears to be less important nowadays than a decade ago, at least where it considers land cover and elevation data. Yet, it remains difficult to decide which data source to use for each application. It is not always evident which data are most cost-effective for a specific purpose and moreover, there is often no information available on the implications of data choice on the accuracy of model output. Furthermore, with the seemingly increased data availability the risk of data misuse

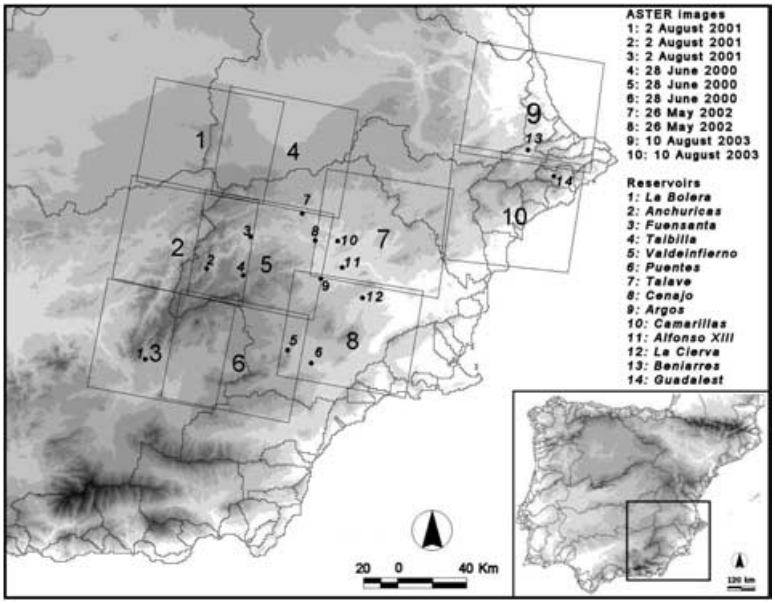

Figure 1. Location of the TERRA-ASTER images and the reservoirs of the 14 catchments for which the WATEM-SEDEM model was applied. In the background elevation is illustrated by the SRTM DEM.

increases. Therefore, the objective of this paper is to assess the impact of different remote sensing-derived sources of input data on model outcomes and to assess the potential of commonly used low-cost data sets as a cost-effective source of information for regional environmental studies.

To illustrate the effect of input data on model output, the existing soil erosion and sediment yield model WATEM-SEDEM (Van Oost *et al*., 2000; Van Rompaey *et al*., 2001; Verstraeten *et al*., 2002) was applied with different data for land cover and topography as input. Sediment yield predicted by the model was compared with measured reservoir sedimentation data for 14 catchments in south-eastern Spain (Figure 1) covering a total surface area of almost 9000 km^2. The 14 catchments were selected from a published data set of sediment yield for 60 reservoirs (Avendaño Salas *et al*., 1997), since they are relatively close to each other, as such facilitating the preparation of the input data layers. Furthermore, with these catchments a relatively large range in observed sediment yield was covered (93–2616 t km^{-2} yr^{-1}), in an area where erosion problems are widespread (Romero Díaz *et al*., 1992; López-Bermúdez *et al*., 1998).

Land cover data from the European land Cover database CORINE (CLC2000; EEA, 2000) were compared with land cover data from classified satellite images obtained from the Advanced Space-borne Thermal Emission and Reflection Radiometer (ASTER), on-board the TERRA satellite. The accuracy of the Shuttle Radar Topography Mission (SRTM) digital elevation model (DEM) was compared with the accuracy of an automatically extracted DEM from an ASTER stereo pair by comparison of both DEMs with a high-resolution reference DEM. We focused on the SRTM DEM, ASTER images and the CORINE database because they are easily accessible, have a relatively high global coverage, a low price, and are probably among the most obvious data sources for many regional model applications.

Remote sensing data preparation

TERRA – ASTER satellite images

A total of 10 ASTER satellite images were used for land cover classification and automatic extraction of a DEM (Figure 1). ASTER images have a spatial resolution of 15 m in three bands of the visible and near-infrared (VNIR) part of the electromagnetic spectrum. In addition, a near-infrared (NIR) backward looking band, six short wavelength infrared (SWIR) bands, and five thermal infrared (TIR) bands are provided with each image (http://asterweb.jpl.nasa.gov/; Abrams, 2000; Hirano *et al*., 2003). All selected images were spring or summer images and provided a cloud-free view of the whole study area. All images were orthorectified using PCI Orthoengine software (Geomatica, 2003) to a Universal Transverse Mercator (UTM) projection (i.e. zone 30N; Datum: European 1950).

The ASTER near-infrared band 3 and the backward looking band form a stereo pair that allows the generation of a DEM. With these two bands a DEM was automatically extracted using PCI software (Geomatica, 2003). Between 10 and 15 ground control points (GCP) and at least 20 tie-points per image were used for DEM generation. Differential GPS measurements in the field and digital orthophotos at 1 metre resolution were used for selection of the GCPs. The height values for the GCPs were obtained either from the differential GPS measurements or from the height available from the SRTM Shuttle DEM. After DEM extraction the post-processing features in PCI software were used to fill data gaps due to water surfaces and steep cliffs. Although theoretically the ASTER DEM can be created at 15 m resolution, previous studies showed best quality at 30 m resolution (Toutin, 2002; Hirano *et al*., 2003; Cuartero *et al*., 2005; Eckert *et al*., 2005). Therefore, the DEM was resampled to 30 m by bilinear interpolation and a mean filter (3*3) was applied to remove irregularities and small pits. Finally, the ten individual DEMs were mosaiced to form a continuous DEM of the study area.

SRTM DEM

In February 2000 the Shuttle Radar Topography Mission (SRTM) was performed and provided a DEM for large sectors of the earth surface (i.e. between ~60N and 60S; Van Zyl, 2001) using radar interferometry. The SRTM DEM was produced at two resolutions: SRTM-1 at 1 arc-second and SRTM-3 at 3 arc-seconds. The 3-arc second DEM was created by aggregation of the 1-arc second DEM, which is expected to

DOI: 10.1002/esp

reduce random errors but not systematic errors in the DEM. For Europe only the SRTM-3 is freely available from the USGS EROS data centre (http://seamless.usgs.gov/). An absolute vertical accuracy of ±16 m, a horizontal positional accuracy of ±20 m and a relative vertical accuracy of ±6 m were reported for the SRTM-1 DEM (Rabus *et al*., 2003). Different accuracy assessments of the SRTM-3 DEM by comparison with an aerophotogrammetric-extracted DEM reported standard deviations of height differences ranging between 12 and 15 m, with maximum elevation differences of 193 m in steep mountainous terrain (Kääb, 2005).

The SRTM-3 DEM (referred to as SRTM DEM) was downloaded and re-projected to a Universal Transverse Mercator (UTM) projection (i.e. zone 30N; Datum: European 1950) with a spatial resolution of 50 m by bilinear interpolation. As there are some data gaps in the SRTM DEM, especially due to water surfaces and steep cliffs, a mean focal filter (7*7) was applied to the DEM to fill the data gaps. This procedure provided a continuous DEM covering the 14 studied catchments.

DEM comparison and land cover classification

DEM accuracy assessment

The accuracy of the ASTER DEM and the SRTM DEM was assessed by comparing slope gradient maps generated from both DEMs with the slope gradient map obtained from a high-resolution reference DEM (REF DEM). The REF DEM was extracted from the contour lines (contour interval 10 m) of digital topographical maps at scale 1:25·000, covering the catchment of the Taibilla reservoir (Figure 1). The topographical maps were obtained from the Spanish National Geographical Institute (IGN) in digital format. The maps were published between the year 2000 and 2002 and were based on photogrammetric information of a flight in 1998. For erosion assessments slope gradient is the most relevant topographical variable, therefore slope gradient maps were compared rather than elevation. Figure 2 provides a visual comparison of the slope gradient maps of the SRTM DEM, the ASTER DEM and the REF DEM. As is apparent from this figure, there is a wide range of slope gradients within the study catchment and there are clear differences in smoothness, detail and spatial variability between the three DEMs.

Slope gradient maps from the ASTER DEM and the SRTM DEM were generated at 30 and 50 m resolution, respectively. The REF DEM was created with IDRISI software (Eastman, 2003) by conversion of the contour lines to a triangulated irregular network (TIN) and subsequently by TIN interpolation to a raster file format. The REF DEM was created at 10 m resolution. From this DEM a slope gradient map was calculated, and subsequently the slope gradient map was aggregated to 30 and 50 m by bilinear interpolation. In addition, the ASTER slope gradient map was also aggregated to 50 m by bilinear interpolation to analyse the effect of pixel aggregation on accuracy. For the accuracy assessment, the root mean square error (RMSE) and the relative root mean square error (RRMSE) were calculated for each slope gradient map as:

$$RMSE = \sqrt{\frac{1}{n}\sum_{i=1}^{n}\left(REF_i - DEM_i\right)^2} \quad (1)$$

$$RRMSE = \frac{\sqrt{\frac{1}{n}\sum_{i=1}^{n}\left(REF_i - DEM_i\right)^2}}{\frac{1}{n}\sum_{i=1}^{n} REF_i} \quad (2)$$

Here, REF stands for the slope gradient map obtained from the reference DEM, and DEM stands for the slope gradient of the maps obtained from either the ASTER- or the SRTM DEM. The RMSE represents the error in slope gradient in degrees while the RRMSE is independent of units. The smaller the RMSE and the RRMSE value, the more accurate is the slope map.

Table I lists the results of the accuracy assessment of the slope gradient maps of the SRTM and the ASTER DEM. From this comparison it appears that the error of the ASTER slope gradient map is larger than the error of the SRTM slope gradi-

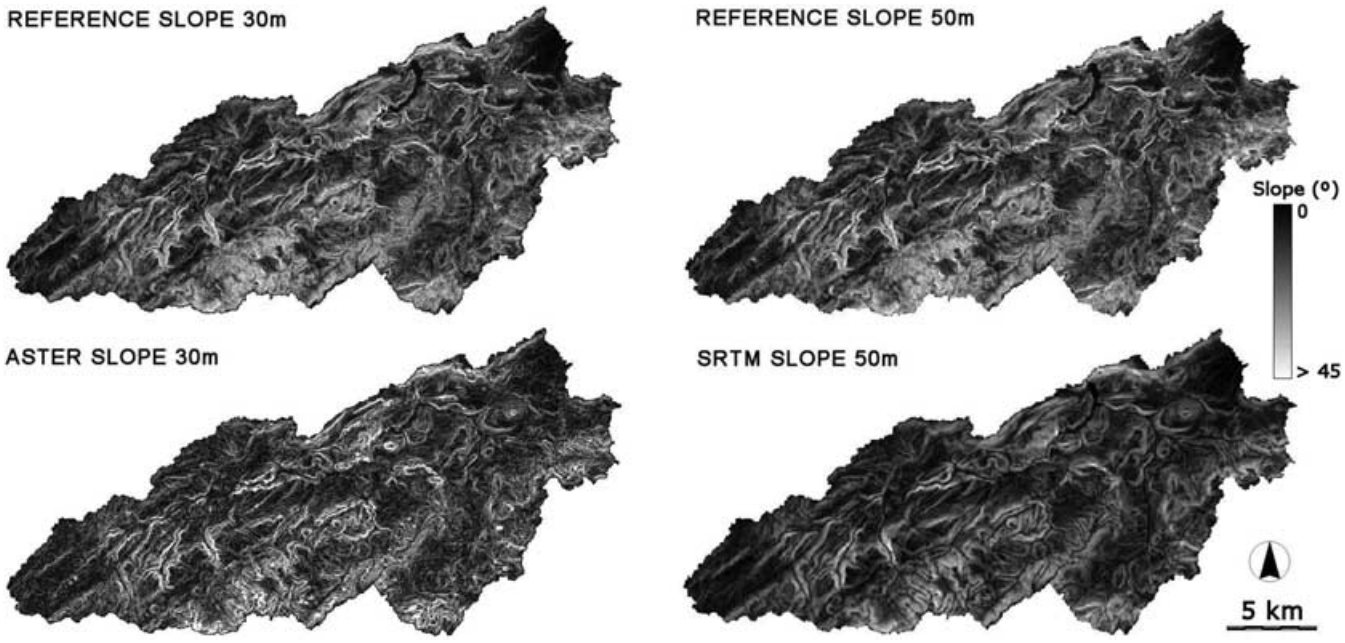

Figure 2. Visual comparison of the slope gradient maps as derived from the ASTER DEM (30 m), the SRTM DEM (50 m), and the reference DEM (30 and 50 m) for the Taibilla catchment.

DOI: 10.1002/esp

Table I. Results of the accuracy assessment of slope gradient maps derived from the ASTER DEM and the SRTM DEM. Slope gradient maps were compared with the slope gradient map obtained from a reference DEM

ASTER DEM 30 m		ASTER DEM 50 m		SRTM DEM 50 m	
RMSE (°)	*RRMSE(–)*	*RMSE (°)*	*RRMSE(–)*	*RMSE(°)*	*RRMSE(–)*
7·2	0·45	7·2	0·44	6·4	0·39

RMSE: Root Mean Square Error; RRMSE: Relative Root Mean Square Error

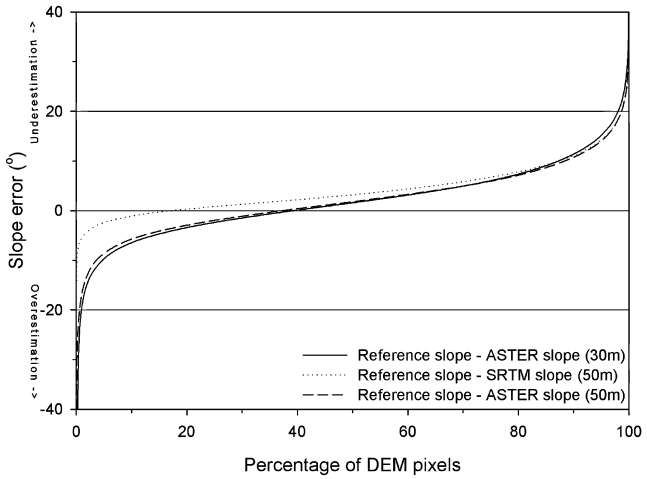

Figure 3. Cumulative frequency diagram of the error in slope gradient as represented by the difference between the slope gradient map of the reference DEM, the SRTM DEM, and the ASTER DEM at either 30 or 50 m resolution.

ent map. Since aggregation of data in the SRTM DEM can explain part of this difference (Van Rompaey *et al*., 1999; Van Rompaey and Govers, 2002) the ASTER-derived slope gradient was also aggregated to 50 m by bilinear interpolation. However, this caused no significant decrease of the error in slope gradient map. The difference between the slope gradient maps is further illustrated in the cumulative frequency diagram of the error in slope gradient (Figure 3). This figure illustrates that both the ASTER and SRTM DEM show more underestimations of slope gradient than overestimations. The ASTER DEM shows more overestimations than the SRTM DEM and also more extreme slope gradient errors in general. Aggregation of the ASTER DEM to 50 m results in some less extreme errors, but there are still significantly more, and more extreme errors than in the SRTM DEM.

ASTER land cover classification and CORINE land cover

A straightforward supervised classification was performed on all ten ASTER images with ERDAS Imagine software (v8·5). Training areas were digitised based on field observations and with the help of digital orthophotos from 1997 and 2000 with a spatial resolution of 1 m, provided by the cartographic service of the regional Ministry of Sustainable Development and Spatial Planning of Murcia. Table II summarises the areas used as training areas for each land cover class. In total about 66 km^2 was used as training area. ASTER images with the same acquisition date (Figure 1) were mosaiced and classified together. Images with a different acquisition date were mosaiced after classification. Finally, a majority filter (3*3) was applied to the full mosaic of all classified images to remove isolated pixels.

Table II. Number of pixels and surface area of training areas used for classification of each land cover class

Land cover class	Number of training pixels	km^2
Arable land	40979	9
Irrigated arable land	11873	3
Almond/Olive orchard	10575	2
Grapes	1050	0
Bare/poorly vegetated	8125	2
Natural grasslands	26780	6
Matorral	54490	12
Coniferous forest	65941	15
Deciduous/Evergreen forest	21125	5
Water surfaces	50826	11
Total	291764	66

Table III. Accuracy and kappa index of agreement (KHAT value) for different band combinations used in the land cover classification of ASTER images

Band combination	Accuracy (%)	KHAT (–)
Bands 1, 2, 3	90	0·88
Bands 1, 2, 3, 4	90	0·88
Bands 1, 2, 3, 4, 5	84	0·81
Bands 1, 2, 3, 4, 5, 6	83	0·80
Bands 1, 2, 3, 4, 5, 6, 7	77	0·73
Bands 1, 2, 3, 4, 5, 6, 7, 8	81	0·78
Bands 1, 2, 3, 4, 5, 6, 7, 8, 9	81	0·78
Bands 2, 3, 4	79	0·75
Bands 1, 2, 3, 4, 8	82	0·79
Bands 1, 2, 3, 4, 5, 8	81	0·78
Bands 1, 2, 3, 4, DEM, ASPECT	67	0·61
Bands 1, 2, 3, 4, DEM	68	0·62
Bands 1, 2, 3, 4, ASPECT	85	0·82

In order to select the optimal band combination for land cover classification, the classification was repeated using different band combinations of the nine VNIR and SWIR bands. In addition a 'logical channel approach' (Hutchinson, 1982; Florinsky, 1998) was applied by the use of elevation and slope aspect, obtained from the SRTM DEM, as additional bands. Each classification was validated by comparison with reference areas (i.e. different from the training sites used for classification). The validation results of each band combination are listed in Table III. The accuracy refers to the percentage of reference pixels correctly classified. The kappa index of agreement (KHAT value) is a measure for the reduction of the error in a classified image compared with a completely random classification (Cohen, 1960; Congalton, 1991). The KHAT value ranges between 0 and 1, and the higher the number the less random the classification. The combination of bands 1–3 provided the best result. Addition of band 4

DOI: 10.1002/esp

Table IV. Confusion matrix of the land cover classification with ASTER bands 1–4. Shows the number of pixels in each class

	Reference data											
Class Name	1	2	3	4	5	6	7	8	9	10	Total	Reliability (%)
1 Arable land	3722	0	515	53	97	208	254	0	0	0	4849	77
2 Irrigated arable land	0	3711	0	0	0	3	0	0	149	0	3863	96
3 Almond/Olive orchard	7	1	660	47	3	134	6	0	0	0	858	77
4 Grapes	0	0	6	157	0	0	0	0	0	0	163	96
5 Bare/poorly vegetated	0	0	0	0	1341	0	13	0	0	0	1354	99
6 Natural grasslands	0	0	1	0	0	124	49	0	0	0	174	71
7 Matorral	0	1	3	0	30	623	1559	50	0	0	2266	69
8 Coniferous forest	0	0	0	0	0	5	101	3091	0	0	3197	97
9 Deciduous/Evergreen forest	0	0	0	0	0	0	0	0	686	0	686	100
10 Water surfaces	0	0	0	0	0	0	0	0	0	5616	5616	100
Total	3729	3713	1185	257	1471	1097	1982	3141	835	5616	**23026**	
Accuracy (%)	99	99	56	61	91	11	79	98	82	100		**90**

provided the same result, whereas addition of the other bands provided worse classification results. Therefore, it was decided to use bands 1–4 for classification. The poorer classification result with more spectral bands can partly be explained by the fact that the TIR and SWIR bands have a lower resolution and because more information also introduces more 'noise' which blurs the classification.

Table IV shows the confusion matrix of the classification with bands 1–4. Beside the classification accuracy, the matrix indicates the reliability of the classification, which refers to the percentage of pixels classified in a class that is correctly classified (Congalton, 1991). From the matrix it appears that there is some confusion between orchards (almond, olive and grape) and arable land. This is probably due to the fact that orchards with large distance between trees and no understorey have a spectral signature comparable with that of bare arable fields. Another important confusion in the classification occurs between natural grasslands, matorral and coniferous forest. This can be explained by the fact that there is a gradual increase in tree density from open natural grasslands over matorral to dense forest, which complicates identification of clear-cut boundaries.

Visual interpretation of the classification results reveals some additional shortcomings of the classification. First of all, several boundary problems were observed in the mosaic of the classified images. Some abrupt boundaries were present between irrigated- and non-irrigated arable lands. This can be largely explained by the differences in the acquisition dates of the images and differences in irrigation schemes between years and within the season. Another problem is that sometimes there is a small green riparian vegetation zone present along the main rivers, which was erroneously classified as irrigated crop.

The second land cover map used in this study was the CORINE land cover map (CLC2000; EEA, 2000) of the European Environment Agency. CORINE has a resolution of 100 m, and consists of 44 land cover classes, of which about 30 classes actually exist within the study area. The minimum mapping unit applied in CORINE is 25 ha and so the map shows relatively large homogeneous land cover units. Figure 4 illustrates the differences in the land cover map of CORINE compared with the classified ASTER images for the Taibilla catchment. Table V compares the CORINE and the classified ASTER map for the dominant land cover classes in all study catchments. Although there are local differences, in general there is good agreement between the percentages of land cover classes in both maps. For example, the total percentage of arable lands in the CORINE map (41%) is very comparable with the percentage of arable land in the ASTER map (43%). Most of the differences are in catchments in the headwaters of the Segura River, where agricultural fields are often small and so are not identified by CORINE. The largest differences are in the percentage of forest cover, where CORINE in general overestimates forest cover compared with the ASTER map. This is probably due to the classification of Matorral and Natural grassland with low tree densities as forest in the CORINE map.

Although the general pattern of land cover in the ASTER and CORINE land cover maps is comparable, the ASTER land cover pattern is much more fragmented than the CORINE map. This is illustrated by the Fragmentation Index (Monmonier, 1974) as presented in Table V. The mean Fragmentation Index (F) for each catchment was calculated as:

$$F = \left(\sum_{i=1}^{i=m} \left(\frac{n-1}{c-1} \right) \Big/ m \right) \tag{3}$$

where n is the number of different classes, c the number of cells considered in a kernel of 7 by 7 pixels, and m the total number of pixels in the image. The larger the Fragmentation Index, the more fragmented is the land cover pattern. The average F of the ASTER maps (0·041) is clearly higher than the average F of the CORINE maps (0·011). This fragmented land cover pattern of the ASTER map is considered more in agreement with the typical Mediterranean mosaic of land cover classes than the large homogeneous classes in CORINE.

Erosion and sediment yield model application

Introduction

In order to assess the implications of data selection on erosion and sediment yield predictions, the WATEM-SEDEM model was applied with different input data for land cover and elevation. So, the aim was not to develop a 'new' or 'better' erosion model, but rather to assess the impact of data selection on model output for regional modelling studies, with the WATEM-SEDEM model as an example. Therefore, first of all and to analyse the effect of the source of land cover data on model

DOI: 10.1002/esp

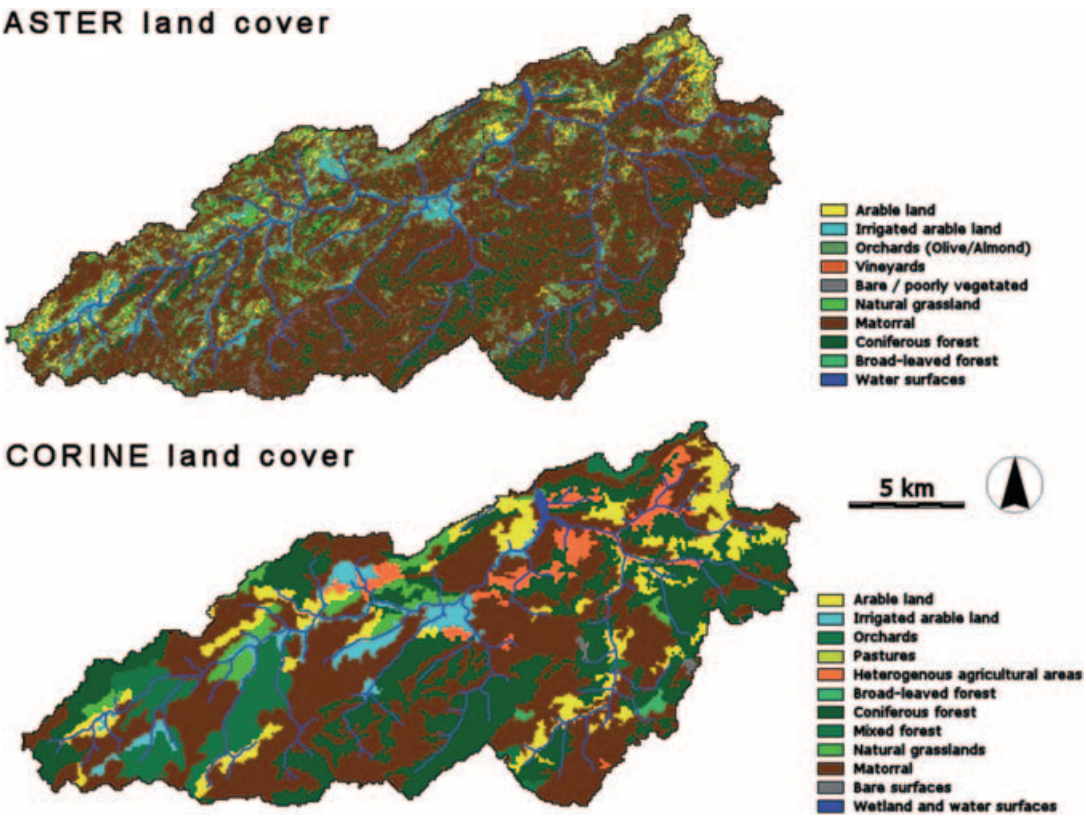

Figure 4. Comparison of the ASTER and CORINE derived land cover map of the Taibilla catchment at 15 and 100 m resolution, respectively. The river network was automatically extracted from the SRTM DEM with a threshold of 1 km^2. This figure is available in colour online at www.interscience.wiley.com/journal/espl

Table V. Comparison of CORINE and ASTER land cover maps by catchment. Indicated are the percentages of each land cover class in both maps and the total for the whole study area

	Arable land total (%)		Forest total (%)		Natural grassland (%)		Matorral (%)		Bare surfaces (%)		Fragmentation#	
Catchment	CORINE	ASTER	CORINE	ASTER	CORINE	ASTER	CORINE	ASTER	CORINE	ASTER	CORINE	ASTER
Alfonso	60	66	14	7	0	1	24	26	2	1	0·010	0·025
Anchuricas	2	15	60	55	8	9	28	14	1	6	0·008	0·060
Argos	39	41	23	13	0	1	34	45	4	1	0·014	0·029
Beniarres	52	48	15	21	0	6	31	25	1	0	0·011	0·048
Bolera	3	17	67	41	0	5	30	27	0	10	0·007	0·066
Camarillas	64	68	7	5	1	5	27	22	1	0	0·010	0·024
Cenajo	31	30	26	17	3	5	40	48	1	0	0·013	0·039
Cierva	49	47	40	21	0	1	11	31	0	0	0·010	0·030
Fuensanta	15	16	39	34	7	7	37	38	3	5	0·010	0·051
Guadalest	35	25	2	21	0	13	63	39	1	2	0·008	0·058
Puentes	55	55	12	6	0	0	24	37	8	2	0·011	0·025
Taibilla	18	21	35	14	3	4	43	60	0	2	0·015	0·046
Talave	22	22	55	43	2	4	18	31	3	0	0·011	0·048
Valdeinfierno	38	45	31	10	1	0	28	40	2	6	0·013	0·030
TOTAL	41	43	25	18	2	4	29	33	2	2	0·011*	0·041*

Fragmentation Index according to Equation (3) (Monmonier, 1974).
* Average Fragmentation Index over all 14 catchments.

predictions, WATEM-SEDEM was calibrated to 14 catchments in south-eastern Spain, using either the ASTER- or the CORINE land cover maps to obtain land cover parameters required for the model. In this analysis the SRTM DEM was used to describe topography since the DEM error analysis demonstrated that the SRTM DEM has a higher accuracy than the ASTER DEM for slope gradient calculation. Measured reservoir sedimentation data were used for calibration of the model. Reservoir sedimentation volumes were measured and published by the 'Centro de Estudios Hidrográficos' (CEH-CEDEX) of the Spanish ministry of the environment using bathymetric reservoir surveys (Avendaño Salas and Cobo Rayán, 1997; Avendaño Salas *et al.*, 1997).

In addition to this analysis and in order to demonstrate the effect of DEM choice on model output, the WATEM-SEDEM model calibrated for the 14 catchments was applied to the drainage basin of the Taibilla reservoir using three different sources of elevation data (REF DEM; ASTER DEM; SRTM DEM)

DOI: 10.1002/esp

and two sources of land cover data (ASTER and CORINE). This was done at various spatial resolutions in order to isolate the effect of spatial resolution on model output. The Taibilla catchment was selected because for this catchment beside the ASTER and SRTM DEM also the REF DEM was available. It is emphasised that this exercise is not a model validation, and the objective of the comparison is not to evaluate the accuracy of model predictions with different input data. Instead, the objective is to evaluate in which way and to what extent different input data affect model output, and to illustrate the importance of model calibration for different data sources of land use and topography.

The WATEM-SEDEM model

The spatially-distributed model WATEM-SEDEM provides estimates of long-term mean annual soil erosion by water as well as of sediment delivery to the river system. The model was originally developed for use in the Loess area of central Belgium (Van Rompaey *et al*., 2001; Verstraeten *et al*., 2002), but since then it has been applied and modified for other environments (Van Rompaey *et al*., 2003; Van Rompaey *et al*., 2005; Verstraeten *et al*., 2007; de Vente *et al*., 2008). The model structure is described in more detail in various earlier publications (Van Oost *et al*., 2000; Van Rompaey *et al*., 2001; Verstraeten *et al*., 2002), so here we confine description to a short summary of model principles and a description of the source of input data.

The WATEM-SEDEM model is pixel-based and consists of a soil erosion assessment, a sediment transport capacity calculation, and sediment routing. Within WATEM-SEDEM mean annual soil erosion by water is predicted with a modified version of the Revised Universal Soil Loss Equation (RUSLE, Renard *et al*., 1997) that was proposed by Desmet and Govers (1996b) as:

$$E = R * K * LS_{2D} * C * P \quad (4)$$

where E is mean annual soil erosion (kg m^{-2} yr^{-1}), R is the rainfall erosivity factor (MJ mm m^{-2} h^{-1} yr^{-1}), K is the soil erodibility factor (kg h MJ^{-1} mm^{-1}), LS_{2D} is the two dimensional topographic factor, C the crop and management factor, and P the erosion control practice factor. In the calculation of the LS_{2D} the unit upslope drainage area is used instead of the original one dimensional linear slope length factor, which allows application to complex 2D landscapes. Moreover, using the 2D calculation of the LS factor, beside sheet and rill erosion, part of the ephemeral gully erosion in the Belgian Loess belt could also be predicted (Desmet *et al*., 1999).

In WATEM-SEDEM an annual sediment transport capacity is calculated on a pixel basis. In this study the transport capacity was calculated as suggested by Verstraeten *et al*. (2007):

$$TC = KTC * R * K * A^{1.4} * S^{1.4} \quad (5)$$

where TC is the transport capacity (kg m^{-2} yr^{-1}), KTC is the transport capacity coefficient used for calibration (-), R and K are the rainfall intensity and the soil erodibility factor of the RUSLE, A is upslope drainage area (m^2), and S is local slope gradient (m m^{-1}). The difference between this equation and the original model formulation (Van Rompaey *et al*., 2001) is that it allows high transport capacity throughout zero-order basins, which is important in basins where ephemeral gully and gully erosion are responsible for a large part of the sediment budget. The transport capacity coefficient (*KTC*) reflects the effects of vegetation cover on sediment transport capacity since, for well vegetated areas, a different *KTC* value was used than for poorly vegetated areas. The *KTC* was used for calibration by applying the model with a wide range of *KTC* values (0–0·1) for the two land cover classes (i.e. well versus poorly vegetated) to find the optimal *KTC* value combination. Sediments were routed through the basin towards the river along runoff paths that are calculated with a multiple-flow algorithm (Desmet and Govers, 1995, 1996a). Sediments are routed through the basin in such a way that sediment deposition is modelled when the *TC* of a pixel is smaller than the sediment flux reaching that pixel. Transport capacity of rivers is assumed to equal sediment load.

Input data

In the calibration of WATEM-SEDEM for the 14 Spanish catchments, the SRTM DEM was used for calculation of slope gradient, upslope area, LS_{2D} factor, and for routing the sediments along a runoff pattern. The SRTM DEM was also used to extract a river network by assuming a channel when the upslope drainage area is larger than 1 km^2, which corresponds roughly with the river network indicated on topographical maps at a scale of 1:200·000. For the Taibilla catchment the calibrated WATEM-SEDEM model was also applied with the ASTER DEM and the REF DEM to provide the topographical variables. The ASTER DEM was prepared at 30 m resolution and aggregated to 50 m by bilinear interpolation. The REF DEM was prepared at 10 m resolution and also aggregated to 50 metres resolution to allow direct comparison with the SRTM DEM results. Pits were removed from all DEMs prior to model application by the pit removal procedure of IDRISI 32.

The CORINE land cover map (CLC2000; EEA, 2000) and the classified ASTER images were used as input to obtain land cover parameters. Since no spatial information on crop rotations is available for all basins, mean RUSLE C values were applied to every land cover category. Table VI lists the C factors per land cover type for both the ASTER and CORINE land cover classes. C factors were assigned to land cover classes based on estimates made in the erosion studies of the Spanish Ministry of the Environment (DGCONA, 2002), and for natural land cover classes using the guidelines proposed by Dissmeyer and Foster (1980). The RUSLE erosion control factor P was set at 1 for all basins since there was no detailed spatially distributed information available on the application of soil conservation measures. Moreover, widely applied conservation measures like reforestation or the construction of check dams in ephemeral channels are not described by the P factor. The effects of reforestation on soil loss are described by the C factor.

The rainfall erosivity factor R was assessed based on mean monthly rainfall data, extracted from the station data of the National Meteorological Institute (INM) for the period 1971–2000 and gridded at 1 km^2. The R factor was calculated from this using the equation proposed by Renard and Freimund (1994). The most detailed soil database available for the whole study area is the European database on soil erodibility at 1 km resolution. This database (ESDBv2 Raster Archive) is freely available from the website of the European Soil Bureau (http://eusoils.jrc.it/). The erodibility map is inferred from soil type, surface fine earth texture and parent material (ESB, 2004). The map consists of five erodibility classes, which, after consulting other erosion studies in Spain for reference values (e.g. ICONA, 1988; DGCONA, 2002), were assigned K values ranging from 10 to 50 (kg h MJ^{-1} mm^{-1}). Analogous to the DEM, all RUSLE input layers (i.e. R, K, C factor) were prepared at 10, 30 and

DOI: 10.1002/esp

Table VI. Overview of the C factors applied in the WATEM-SEDEM model for the CORINE and ASTER land cover maps

Land cover classes	*C* factor CORINE	*C* factor ASTER
Urban areas	0	0
Non-irrigated arable land	0·44	0·44
Irrigated land	0·25	0·25
Rice fields	0·05	–
Orchards	0·35	0·35
Fruit tree plantations	0·30	–
Heterogeneous agricultural areas	0·30	–
Deciduous/evergreen forest	0·002	0·002
Coniferous forest	0·004	0·004
Mixed forest	0·003	–
Natural grassland	0·08	0·08
Shrubs and transitional woodland / Matorral	0·03	0·03
Bare surfaces above 1000 m elevation	0·12	0·12
Water surfaces	0	0

50 m resolution in order to allow application of the model at these three resolutions.

Model results

WATEM-SEDEM was first calibrated for the 14 study catchments by varying *KTC* in Equation (5) for two contrasting land cover categories, reflecting their different sensitivity to overland flow sediment transport. For well-vegetated surfaces (i.e. natural vegetation classes) a low *KTC* value was used, and for poorly-vegetated surfaces (i.e. arable land and bare surfaces) a high *KTC* value was applied. This allows more sediment transport on poorly vegetated areas than on well vegetated areas. For each catchment WATEM-SEDEM was run with a wide range of KTC-values with either ASTER or CORINE as land cover data. For each parameter combination (*KTC HIGH* and *KTC LOW*), the absolute sediment yield (*SY*; t yr^{-1}) and area-specific sediment yield (*SSY*; t km^{-2} yr^{-1}) were calculated for each catchment since calibration for *SY* and *SSY* will provide different results (de Vente *et al*., 2008). The optimal combination of *KTC* values for either *SS*Y or *SY* was selected using the Nash and Sutcliffe (1970) model efficiency (*ME*):

$$ME = 1 - \frac{\sum_{i=1}^{n} (O_i - P_i)^2}{\sum_{i=1}^{n} (O_i - O_{mean})^2} \quad (5)$$

where O_i is the observed value, P_i is the predicted value and O_{mean} the mean observed value. The *ME* ranges from $-\infty$ to 1, the closer the *ME* approaches 1, the more efficient the model is.

Figures 5 and 6 show the calibration curves for *SSY* and *SY* after application of the model to 14 basins in south-eastern Spain using either ASTER or CORINE land cover data as input. In all cases the SRTM DEM was used to describe topography. Table VII summarises the optimal *KTC* values and corresponding model efficiencies. In general calibration results were comparable but slightly better for *SY* than for *SSY*, and *ME* was slightly higher with CORINE than when ASTER data were used to describe land cover characteristics. This can also be seen in Figure 7, where predicted and observed sediment yield are plotted for both model applications. When calibrated for *SY*, *KTC HIGH* is almost two times higher with ASTER land cover than with CORINE land cover, whereas *KTC LOW* with CORINE is twice the *KTC LOW* calibrated with ASTER land cover. Likewise, when calibrated for *SSY*, *KTC HIGH* is just over two times higher with ASTER than with CORINE land cover. Remarkably the optimal value of *KTC LOW* with ASTER land use is zero, meaning that there is no sediment export from well-vegetated areas.

It is apparent from Figure 7 that there is one catchment (Fuensanta) with an extremely high absolute sediment yield *SY* that strongly affects model results. Calibration for *SY* without this observation results in a model with an R^2 between predicted and observed values of 0·41 and 0·22 for ASTER and CORINE landcover respectively. However, the *SY* of this catchment is not an extreme value within the total data set of 60 Spanish catchments where the sediment yield data were extracted from, neither is it an extreme value for area-specific sediment yield. Therefore, it was decided not to remove this observation from the database.

After calibration of WATEM-SEDEM for the 14 study catchments, the calibrated model was applied to the Taibilla catchment with different DEMs to describe topography in order to illustrate the effect of DEM source and resolution as well as land cover combinations on the predicted sediment yield and on sediment connectivity. Table VIII shows the sediment yield prediction and Figure 8 shows the spatial pattern of erosion and deposition prediction for the different DEM and land cover combinations. It is emphasised that Table VIII and Figure 8 present a comparison of model output with different input data and are not intended as a validation of the model or of the input data. WATEM-SEDEM was only calibrated with the SRTM DEM. The objective of this comparison is therefore not to evaluate the accuracy of model predictions of catchment sediment yield with different input data, and it is not the intention to conclude if WATEM-SEDEM predictions with the SRTM DEM are better than with an ASTER DEM or vice versa. The results do show however how DEM source and resolution considerably affect model output. This is considered of interest because it provides insight into how transport capacity and sediment connectivity are affected by the different DEMs and resolutions and how this interacts with different land cover maps.

First of all, it can be seen that predictions with the ASTER DEM (50 m) and the REF DEM (50 m) are comparable, but higher than predictions with the SRTM DEM. The sediment yield predictions with CORINE land cover are overall somewhat higher than with ASTER land cover. Figure 8 also reflects the more fragmented land cover of the ASTER map compared with CORINE land cover that consists of larger homogeneous land units. Although there are some spatial differences and large differences in absolute values, the major sources and

DOI: 10.1002/esp

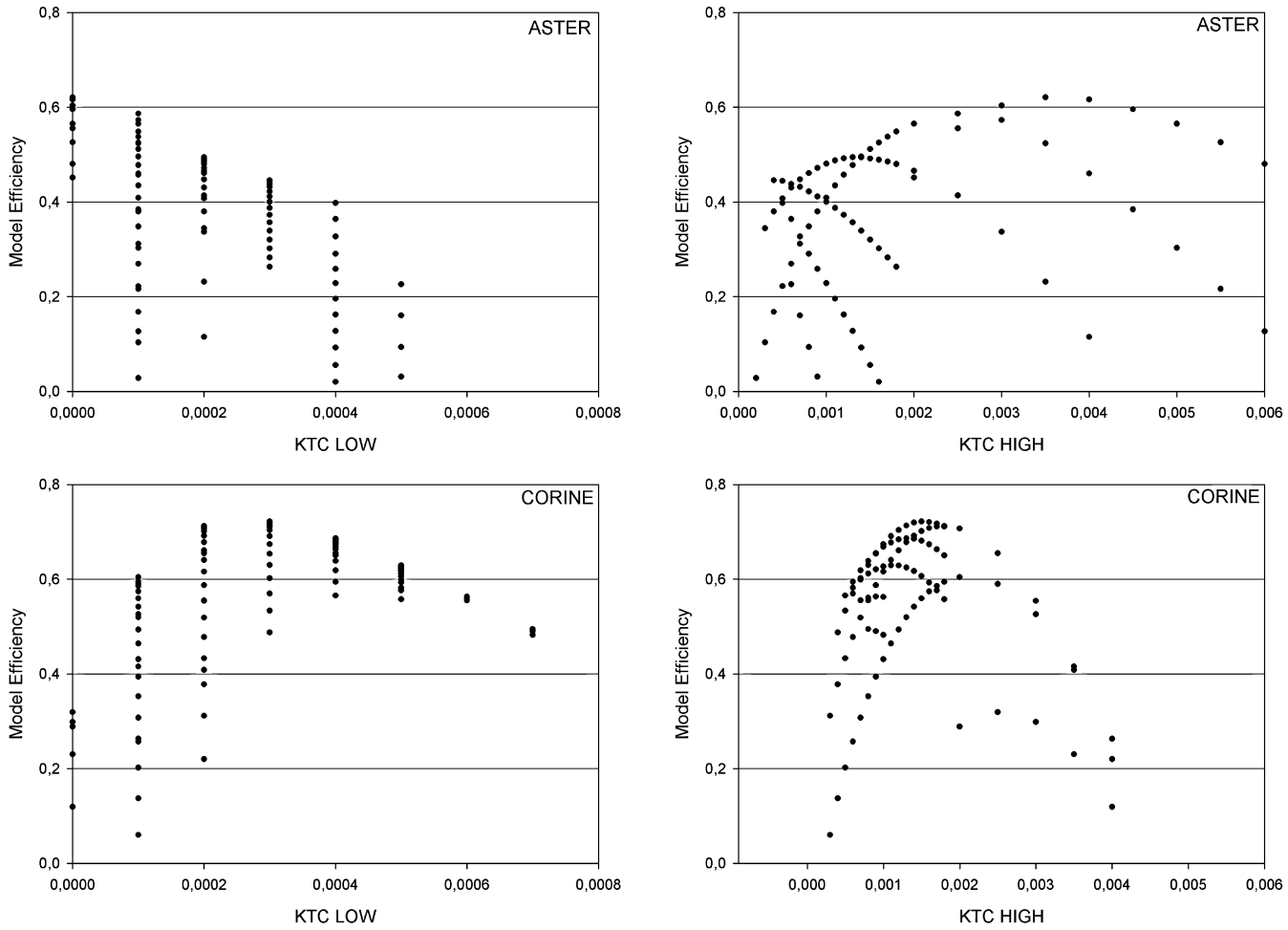

Figure 5. WATEM-SEDEM calibration curves of *KTC HIGH* and *KTC LOW* for area-specific sediment yield (*SSY*) with either ASTER or CORINE land cover maps as input.

sinks of sediment within the basin are comparable for all three DEMs at 50 m resolution, with either ASTER or CORINE as land cover data source.

It is remarkable that better agreement was found with measured sediment yield with the 30 m ASTER DEM than with the SRTM DEM, although *KTC* values were calibrated with the SRTM DEM. Furthermore, the predictions with the ASTER DEM (30 m) and the REF DEM (10 m) are notably lower than the predictions with either the SRTM DEM or the REF DEM at 50 m. So, an increased DEM resolution results in a decrease of predicted sediment yield. This shows the scale dependency of the *KTC* value and implies that the model needs to be recalibrated for application at any new resolution and for each data source.

Discussion

DEM selection

Compared with the reference DEM the SRTM DEM provided better accuracy of slope gradient than the ASTER DEM. Overall, the SRTM and ASTER DEM underestimated slope gradient compared with the reference DEM, although overestimations were also present. While the advantage of the ASTER DEM is that its spatial resolution is higher, so that it potentially contains more detail, it appeared that there are more extreme over- and underestimations of slope gradient with the ASTER DEM than with the SRTM DEM. This is in agreement with Kääb (2005) who found that the SRTM DEM contained less large errors than an ASTER derived DEM. On the other hand, in a comparison of the SRTM DEM (90 m) with high-resolution data (10 m) and high-resolution data degraded to 90 m, Hancock *et al* (2006) concluded that the lack of detail in lower resolution DEMs in general is reflected in a poor representation of hillslope curvature, catchment area, relief and shape. However, area–slope and area–elevation (hypsometry) properties were well depicted by the DEMs at 90 m resolution. Therefore, Hancock *et al*. (2006) recommend the use of the SRTM DEM especially for qualitative assessments of large catchments, whereas quantitative assessment of catchment hydrology or geomorphology should be performed carefully.

An important advantage of the SRTM DEM is that it can be downloaded free of charge and that it requires very little preprocessing except for missing data of water surfaces and steep cliffs in mountainous terrain. For small data gaps this can easily be solved by application of a mean focal filter as was done in this study. For larger data gaps merging with the elevation data from other sources, for example an ASTER derived DEM can provide a solution (Kääb, 2005). The ASTER images are relatively cheap (~80 US Dollar per scene in 2007) however, the preparation of an ASTER DEM requires important pre-processing, specialised software and sufficient high-quality GCPs. Another complication when using the ASTER

DOI: 10.1002/esp

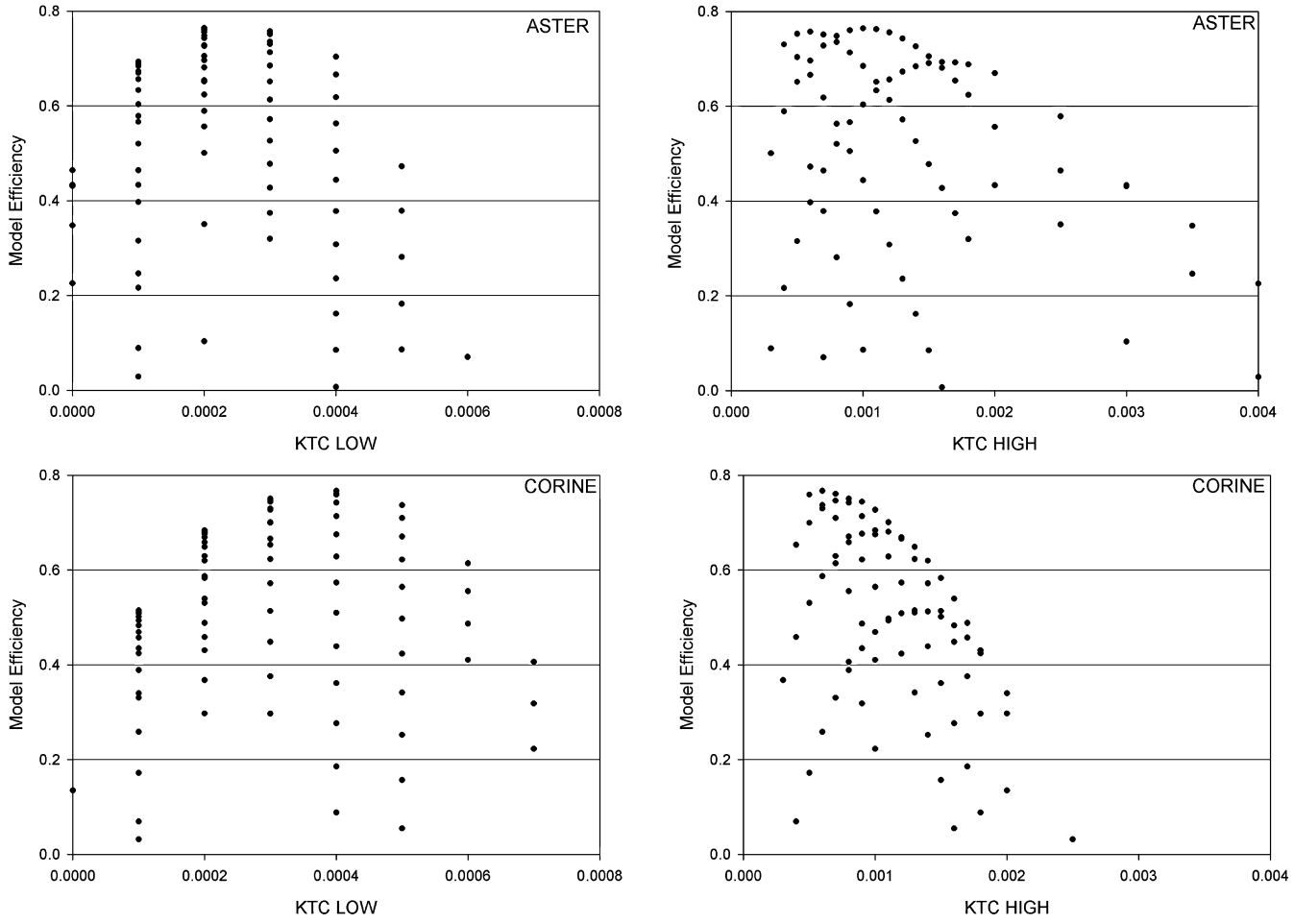

Figure 6. WATEM-SEDEM calibration curves of *KTC HIGH* and *KTC LOW* for absolute sediment yield (*SY*) with either ASTER or CORINE land cover maps as input.

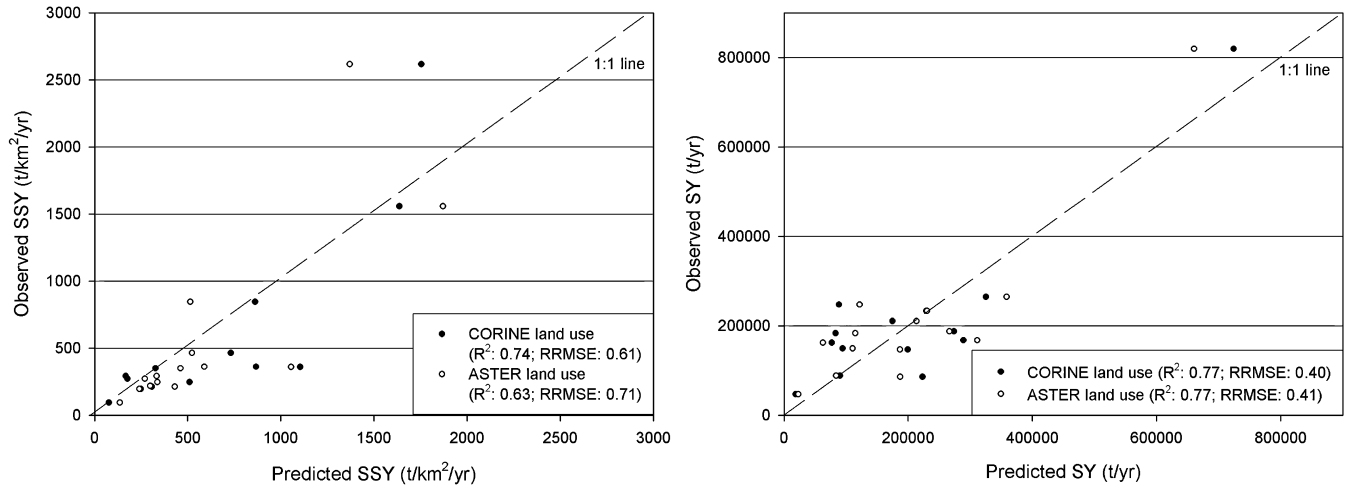

Figure 7. A comparison of predicted and observed area-specific sediment yield (*SSY*) and absolute sediment yield (*SY*) with either CORINE or ASTER land cover maps as input.

Table VII. Overview of the optimal *KTC* values and corresponding model efficiencies (*ME*) for area-specific (*SSY*; t km^{-2} yr^{-1}) and absolute sediment yield (*SY*; t yr^{-1}).

	ASTER		CORINE	
	SSY	*SY*	*SSY*	*SY*
KTC LOW ×10^4	0	2	3	4
KTC HIGH ×10^4	35	10	15	6
ME	0·62	0·76	0·72	0·77

DEM for large continuous areas is the presence of small elevation differences between the DEMs of the individual images, causing elevation steps at the image borders. This problem can be reduced by the selection of more GCPs with a high level of accuracy. However, it is often not easy to find clearly recognisable GCPs. Therefore, notwithstanding the lack of detail compared with a high-resolution DEM, and given that a high-resolution DEM is often not available, it is concluded that the SRTM DEM provides the most feasible source of information of topography for regional- or global-scale model application.

DOI: 10.1002/esp

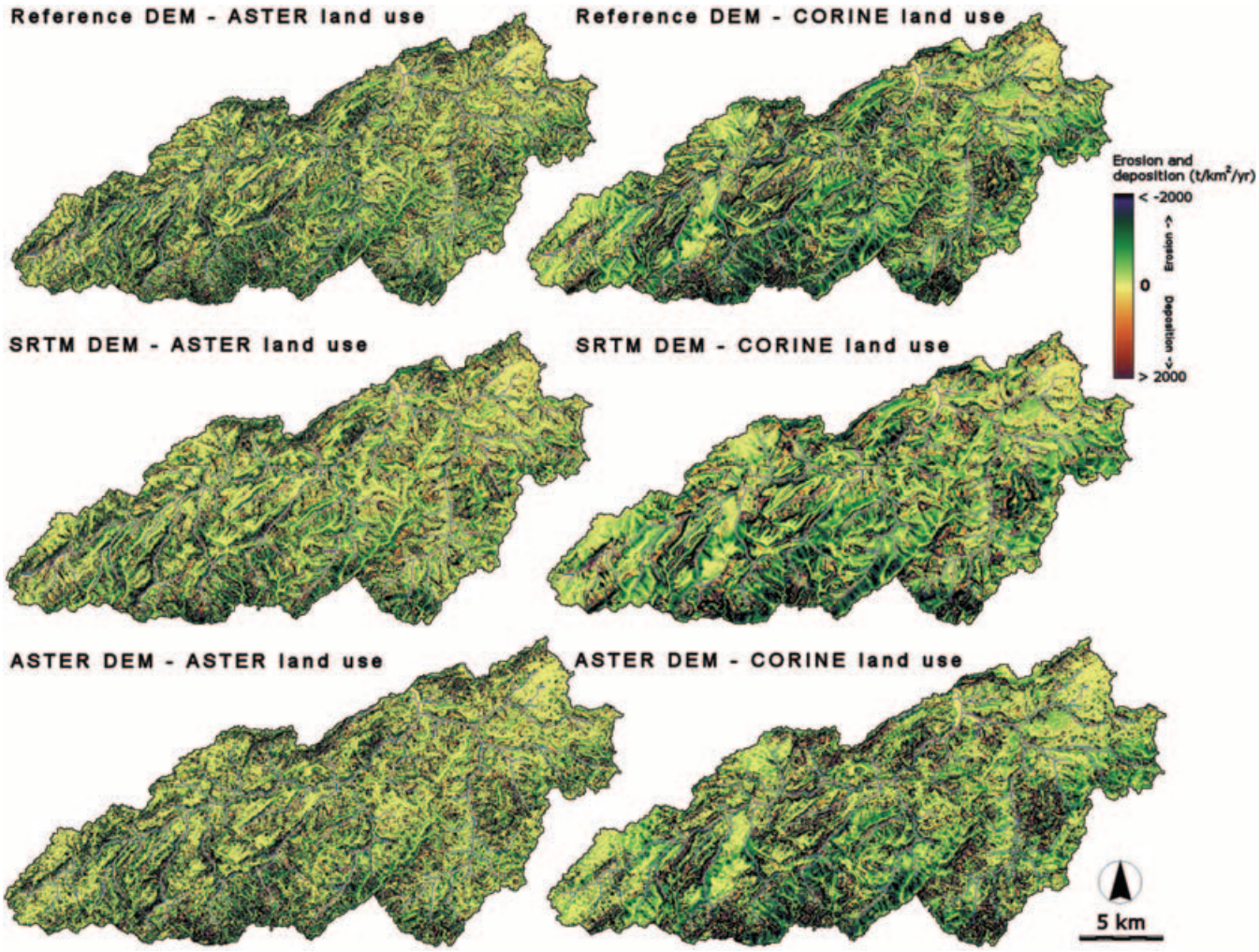

Figure 8. Spatial patterns of predicted soil erosion and sediment deposition by WATEM-SEDEM with different combinations of DEM and land cover as input for the Taibilla catchment. All examples are at 50 m resolution and with optimal *KTC* values for absolute sediment yield. This figure is available in colour online at www.interscience.wiley.com/journal/espl

Table VIII. Comparison of area-specific sediment yield (*SSY*; t km^{-2} yr^{-1}) and absolute sediment yield (*SY*; 1000 t yr^{-1}) prediction for the Taibilla catchment with different land cover and DEM combinations. All predictions are made with the optimal *KTC* values (*HIGH/LOW*) calibrated for the 14 study catchments with the SRTM DEM and either ASTER or CORINE land cover as input. Also indicated is the mean upslope drainage area per pixel (*A*) for each DEM.

DEM source	SRTM 50 m	REF 50 m	REF 10 m	ASTER 50 m	ASTER 30 m
SSY with ASTER land cover (*KTC*: 0·0035/0)	521	596	165	588	436
% of observed *SSY*	112	129	36	127	94
SSY with CORINE land cover (KTC: 0·0015/0·0003)	755	955	150	916	612
% of observed *SSY*	163	206	32	198	132
SY with ASTER land cover (*KTC*: 0·001/0·0002)	188	237	42	225	131
% of observed *SY*	128	162	29	153	89
SY with CORINE land cover (*KTC*: 0·0006/0·0004)	204	259	38	244	159
% of observed *SY*	139	177	26	167	108
Mean upslope area (*A*, km^2)	9	9	8	6	5

SRTM: SRTM DEM; REF: Reference DEM; ASTER: ASTER DEM
The underlined data refer to calibrated values.

Land cover data

Classification of the ASTER images provided a relatively reliable land cover map with an estimated accuracy of 90%. Although the ASTER land cover map shows significantly more detail and although there are local differences, the large-scale pattern of land cover is in agreement with the CORINE land cover maps. The most important difference is that the ASTER land cover shows a much more fragmented landscape than the CORINE land cover, since small patches of vegetation or arable land (<25 ha) are not represented on the CORINE land cover map. On the other hand, the CORINE map distinguishes

DOI: 10.1002/esp

more land cover classes than were identified in the current ASTER land cover classification.

The CORINE land cover database can be downloaded free of charge, but has the limitation that it is only available for Europe and most likely will be updated approximately every 10 years. Conversely, ASTER images are not free, but have a world-wide coverage and allow annual or even monthly updates of land cover if required. The most important problem for the ASTER land cover classification was compilation of the mosaic due to differences in the acquisition dates of the separate images, which caused differences in the identification of irrigated crops. This problem can probably be solved by application of a multi-temporal classification instead of the current single date classification. Another part of the classification that might be enhanced is the identification of different vegetation density classes between natural grassland, Matorral and forest. This might be achieved by a stratified classification and possibly by the use of a vegetation index such as the Normalised Difference Vegetation Index (NDVI). For the current application however, this was not considered priority as most erosion occurs on arable lands and differences between the C factors and erosion rates for natural vegetation classes are relatively low.

Implications of data selection for regional erosion and sediment yield prediction

The increased availability of spatial data sources of topography and land cover with a global coverage offers a new opportunity for application of all kinds of environmental models. This study demonstrates that the use of SRTM or ASTER data for topography, and CORINE or ASTER-derived land cover data can provide reasonable results for prediction of sediment yield at the catchment scale. However, there are some limitations with respect to the quality and detail of the data, and interpretation of model results should be done carefully.

First of all, the current results show that WATEM-SEDEM is a scale-dependent model since not only DEM source, but also DEM resolution strongly affects model output. For example, the predicted sediment yield with any of the DEMs at 50 m resolution was much higher than when the ASTER DEM (30 m) or the REF DEM (10 m) were used (see Table VIII). This is surprising since coarse-resolution DEMs in general underestimate slope gradient compared with high-resolution DEMs (Zhang *et al*., 1999), and so a lower sediment yield would be expected with the SRTM DEM than with the ASTER DEM (30 m) or with the REF DEM (10 m). This is also in contrast with Van Rompaey *et al*. (2001) who found that the WATEM-SEDEM predicted sediment yield decreased with decreasing DEM resolution due to decreasing mean slope gradients. However, comparable results were reported by Verstraeten (2006) who applied the WATEM-SEDEM model to the drainage basin of the Scheldt River and predicted higher sediment yield with the SRTM DEM than with a reference DEM (20 m). Verstraeten (2006) explained this by the fact that due to random errors, the average slope gradient of the SRTM DEM for low slope gradient classes is higher than for the reference DEM. Moreover, at a lower DEM resolution low slope gradients are combined, which leads to steeper slopes in low slope categories, and therefore with the SRTM DEM less sediment deposition will be predicted at the footslopes close to the river channel (Verstraeten, 2006; de Vente, 2009). Apart from differences in slope gradient, this scale effect can probably be explained by artefacts in the high- resolution DEMs. The high-resolution DEMs are less smooth than the low- resolution DEMs, and irregularities and pits cause errors in upslope area calculation (Table VIII), and elevation steps ('terraces') on steep slopes that trap sediments. Although pits were removed, some pits were so large that they hampered proper calculation of upslope area in WATEM-SEDEM. The underestimation of upslope drainage area results in a lower erosion rate (Equation (4)) and transport capacity (Equation (5)), and so in lower predicted sediment yield. The underestimation of upslope area due to pits appears to be a problem especially in the ASTER DEM (see Table VIII), and is probably an artefact of vegetation that was not filtered out of the DEM. The presence of steps on steep slopes explains the low predicted sediment yield with the REF DEM (10 m). For the ASTER and REF DEM aggregation to a lower resolution resulted in a smoother DEM and in a higher predicted sediment yield. On the other hand, underestimation of slope gradient in the lower resolution DEMs resulted in a lower predicted sediment yield with the SRTM DEM than with the ASTER (50 m) and REF DEM (50 m).

Scale dependency is not limited to the WATEM-SEDEM model but is a general characteristic of spatially distributed models. Also for various physics-based models an important effect of DEM resolution on erosion and sedimentation calculations was reported (Schoorl *et al*., 2000; Renschler and Harbor, 2002; Chaplot, 2005; Hancock *et al*., 2006). For example, more runoff, erosion and sediment yield was predicted by the WEPP model with a low-resolution DEM than with a high-resolution DEM (Renschler and Harbor, 2002), and in an application of the SIBERIA landscape evolution model, the calibrated sediment transport parameter was almost five times higher with a high-resolution DEM (10 m) than with the low-resolution SRTM DEM (90 m) (Hancock *et al*., 2006). Nevertheless, the authors concluded that the SRTM DEM results in relatively low, but reasonable erosion predictions when compared with field measurements, although the spatial pattern of erosion was more accurately predicted by high-resolution elevation data than by the SRTM DEM.

When interpreting model results it is important to realise that an accurate prediction of sediment yield at the catchment scale does not necessarily imply that the spatial patterns of sources and sinks of sediment are also accurately predicted (Takken *et al*., 1999, 2005; Vigiak *et al*., 2006). This is nicely illustrated by the fact that the prediction of sediment yield in the Taibilla catchment using the ASTER DEM (30 m) provided better results than with the SRTM DEM (Table VIII), although the ASTER DEM gives a less accurate representation of slope gradient than the SRTM DEM, and underestimated upslope area. So, with a relatively low quality DEM fairly good predictions of sediment yield can be obtained, while the absolute values of erosion and sediment deposition estimates within the catchment are probably erroneous.

Beside the DEM source and resolution, the spatial organisation of land cover classes is important in the assessment of transport capacity within a landscape (Van Oost *et al*., 2000; Bakker *et al*., 2008). This explains the difference in the optimal transport capacity coefficient, KTC, values with ASTER or CORINE land cover. In the patchy, fragmented, vegetation cover of the ASTER map more sediment from arable fields will be trapped on non-arable land, and therefore the *KTC* value of arable land is higher with ASTER land cover than with CORINE. In other words, the CORINE land cover map results in higher sediment connectivity of the landscape than with the ASTER land cover map. Obviously, these differences influence the *modelled* spatial patterns and magnitude of sources and sinks of sediment. Validation of these patterns requires more research, for example detailed field mapping or comparison of model results with measured sediment yield within the catchment.

DOI: 10.1002/esp

Although model calibration is required for each source of elevation and land cover data, the large-scale patterns of predicted sources and sinks of sediment are similar for the different data combinations used (Figure 8). Renschler and Harbor (2002) similarly concluded that although the use of commonly available topographic data affects the output of the WEPP erosion model, the large-scale patterns of predicted soil erosion and sediment yield are similar to those with high-resolution data, and can be useful in decision support regarding soil and water conservation.

Conclusions

This study shows that there are important differences in the accuracy, detail and type of information provided on topography and land cover by different remote sensing derived data sources. Regarding topography, the SRTM DEM is considered a more feasible data source for regional model applications than the ASTER DEM due to its better estimates of slope gradient and upslope area, its lower price and limited pre-processing. For land cover, the ASTER land cover map shows a much more fragmented land cover pattern than the CORINE (CLC 2000) map, although the large-scale pattern of land cover is comparable in both maps. For the present erosion and sediment yield assessment the ASTER land cover was considered more appropriate since the spatial structure of land cover is more relevant than the number of identified land cover classes.

After model calibration, the use of the SRTM or ASTER DEM in combination with either ASTER or CORINE derived land cover information allows a relatively accurate prediction of sediment yield at the catchment scale with WATEM-SEDEM. Connectivity is higher with CORINE than with the ASTER land cover maps due to the less fragmented landscape in CORINE compared with ASTER.

In spite of the overall underestimation of slope gradient by the low-resolution DEMs, the model predicted higher sediment yields with a low-resolution DEM than with a high-resolution DEM with the same *KTC*. This can be attributed to a smoother topography with fewer pits, and to a higher slope estimate for low slope categories in the low resolution DEMs. This insinuates a higher connectivity of the low-resolution DEMs compared with the high-resolution DEMs. In conclusion, since both source and resolution of the data affect model output, model calibration is required for each data source and resolution used.

Although absolute values of predicted erosion and sediment deposition rates change, differences in the predicted large-scale patterns of sources and sinks of sediment are relatively small for the different input data used. So, for large-scale qualitative assessment and for prediction of sediment yield at the catchment scale, either CORINE or ASTER derived land cover in combination with the SRTM DEM or ASTER DEM can provide reliable and useful results. For more detailed quantitative spatially-distributed assessments, the SRTM DEM in combination with ASTER derived land cover information will probably provide best results. However, given the overall underestimation of slope gradient and the lack of detail in low-resolution DEMs in general, the validation of the spatial pattern of predicted erosion and sediment deposition rates requires further research.

Acknowledgements—We thank the Geology department of the Africa Museum, and especially Max Fernandez and Johan Lavreau for assisting with the ASTER DEM extraction. We also thank Veronique De Laet for discussions and cooperation in DEM generation and image pre-processing. The EEZA-CSIC in Almeria kindly provided gridded mean monthly rainfall data for Spain. We are grateful to colleagues at the CEBAS-CSIC for their hospitality, help and interest in this research. The research described in this paper was conducted in the framework of the EC-DG RTD- 6th Framework Research Programme (sub-priority 1·1·6·3) -Research on Desertification- project DESIRE (037046): Desertification Mitigation and Remediation of land – a global approach for local solutions. The first author also acknowledges financial support from the SENECA foundation.

References

Abrams M. 2000. The advanced spaceborn thermal emission and reflection radiometer (ASTER): data products for the high spatial resolution imager on NASA's Terra platform. *International Journal of Remote Sensing*. **21**(5): 847–859.

Avendaño Salas C, Cobo Rayán R. 1997. Metodología para estimar la erosion de cuencas fluviales a partir de la batimetría de embalses. In *El paisaje mediterráneo a través del espacio y del tiempo. Implicaciones en la desertificación*, Ibáñez JJ, Valero Garcés BL, Machado C (eds). Geoforma Ediciones: Logroño; 239–257.

Avendaño Salas C, Sanz Montero E, Gómez Montaña JL. 1997. Sediment yield at Spanish reservoirs and its relationship with the drainage basin area. In *Dix-neuvième Congrès des Grands Barrages. Commission Internationale De Grands Barrages*, Florence; 863–874.

Bakker MM, Govers G, van Doorn A, Quetier F, Chouvardas D, Rounsevell M. 2008. The response of soil erosion and sediment export to land-use change in four areas of Europe: the importance of landscape pattern. *Geomorphology*. **98**(3–4): 213–226.

Chaplot V. 2005. Impact of DEM mesh size and soil map scale on SWAT runoff, sediment, and NO3-N loads predictions. *Journal of Hydrology* **312**(1–4): 207–222.

Cohen J. 1960. A coefficient of agreement of nominal scales. *Educational and Psychological Measurement* **20**(1): 37–46.

Congalton RG. 1991. A review of assessing the accuracy of classifications of remotely sensed data. *Remote Sensing of Environment* **37**(1): 35–46.

Cuartero A, Felicisimo AM, Ariza FJ. 2005. Accuracy, reliability, and depuration of SPOT HRV and Terra ASTER digital elevation models. *IEEE Transactions on Geoscience and Remote Sensing* **43**(2): 404–407.

de Vente J. 2009. Soil erosion and sediment yield in mediterranean geoecosystems. Scale issues, modelling and understanding. PhD thesis, K.U.Leuven, Leuven.

de Vente J, Poesen J. 2005. Predicting soil erosion and sediment yield at the basin scale: scale issues and semi-quantitative models. *Earth-Science Reviews* **71**(1–2): 95–125.

de Vente J, Poesen J, Verstraeten G, Van Rompaey A, Govers G. 2008. Spatially distributed modelling of soil erosion and sediment yield at regional scales in Spain. *Global and Planetary Change* **60**(3–4): 393–415.

Desmet PJJ, Govers G. 1995. GIS-based simulation of erosion and deposition patterns in an agricultural landscape: a comparison of model results with soil map information. *CATENA* **25**(1–4): 389–401.

Desmet PJJ, Govers G. 1996a. Comparison of routing algorithms for digital terrain models and their implications for predicting ephemeral gullies. *International Journal of Geographic Information Science* **10**: 311–331.

Desmet PJJ, Govers G. 1996b. A GIS procedure for the automated calculation of the USLE LS-factor on topographically complex landscape units. *Journal of Soil and Water Conservation*. **51**: 427–433.

Desmet PJJ, Poesen J, Govers G, Vandaele K. 1999. Importance of slope gradient and contributing area for optimal prediction of the initiation and trajectory of ephemeral gullies. *CATENA* **37**(3–4): 377–392.

DGCONA. 2002. Inventario Nacional de Erosión de Suelos 2002–2012. Región de Murcia. Dirección General de Conservación de la Naturaleza, Ministerio de Medio Ambiente, Murcia.

Dissmeyer GE, Foster GR. 1980. A guide for predicting sheet and rill erosion on forest land. Technical Publication SA-TP-11, USDA forest service-State and private forestry Southeastern area.

Eastman JR. 2003. *IDRISI Kilimanjaro Guide to GIS and Image Processing*. Clark Labs: Worcester.

Eckert S, Kellenberger T, Itten K. 2005. Accuracy assessment of automatically derived digital elevation models from ASTER data in mountainous terrain. *International Journal of Remote Sensing* **26**(9): 1943–1957.

EEA. 2000. CORINE land cover 2000. European Environment Agency http://image2000.jrc.it.

ESB. 2004. European Soil Database. European Soil Bureau Network and the European Commission, EUR 19945 EN, http://eusoils.jrc.it.

Florinsky, I.V., 1998. Combined analysis of digital terrain models and remotely sensed data in landscape investigations. *Progress in Physical Geography* **22**(1): 33–60.

Geomatica, 2003. *GEOMATICA ORTHOENGINE USERGUIDE*, Version 9·0. PCI Geomatics: Richmond Hill.

Hancock GR, Martinez C, Evans KG, Moliere DR. 2006. A comparison of SRTM and high-resolution digital elevation models and their use in catchment geomorphology and hydrology: Australian examples. *Earth Surface Processes and Landforms* **31**(11): 1394–1412.

Hirano A, Welch R, Lang H. 2003. Mapping from ASTER stereo image data: DEM validation and accuracy assessment. *ISPRS Journal of Photogrammetry and Remote Sensing* **57**(5–6): 356–370.

Hutchinson CF. 1982. Techniques for combining Landsat and ancillary data for digital classification improvement. *Photogrammetric Engineering and Remote Sensing* **48**(1): 123–130.

ICONA. 1988. Mapas de Estados Erosivos. Cuenca hidrográfica del Segura. Instituto Nacional para la Conservación de la Naturaleza (ICONA), Minesterio de agricultura, pesca y alimentación, Madrid.

Kääb A. 2005. Combination of SRTM3 and repeat ASTER data for deriving alpine glacier flow velocities in the Bhutan Himalaya. *Remote Sensing of Environment* **94**(4): 463–474.

López-Bermúdez F, Romero-Diaz A, Martinez-Fernandez J, Martinez-Fernandez J. 1998. Vegetation and soil erosion under a semi-arid Mediterranean climate: a case study from Murcia (Spain). *Geomorphology* **24**(1): 51–58.

Merritt WS, Letcher RA, Jakeman AJ. 2003. A review of erosion and sediment transport models. *Environmental Modelling & Software* **18**(8–9): 761–799.

Monmonier MS. 1974. Measures of pattern complexity for choropleth maps. *The American Cartographer* **2**: 159–169.

Nash JE, Sutcliffe JV. 1970. River flow forecasting through conceptual models part I – a discussion of principles. *Journal of Hydrology* **10**: 282–290.

Rabus B, Eineder M, Roth A, Bamler R. 2003. The shuttle radar topography mission–a new class of digital elevation models acquired by spaceborne radar. *ISPRS Journal of Photogrammetry and Remote Sensing* **57**(4): 241–262.

Renard KG, Freimund JR. 1994. Using monthly precipitation data to estimate the R-factor in the revised USLE. *Journal of Hydrology* **157**: 287–306.

Renard KG, Foster GR, Weesies GA, McCool DK, Yoder DC. 1997. Predicting soil erosion by water: a guide to conservation planning with the revised universal soil loss equation (RUSLE). *Agriculture Handbook*, *703*. US Department of Agriculture: Washington DC.

Renschler CS, Harbor J. 2002. Soil erosion assessment tools from point to regional scales – the role of geomorphologists in land management research and implementation. *Geomorphology* **47**(2–4): 189–209.

Romero Díaz MA, Cabezas F, López Bermúdez F. 1992. Erosion and fluvial sedimentation in the River Segura Basin (Spain). *Catena* **19**: 379–392.

Schoorl JM, Sonneveld MPW, Veldkamp A. 2000. Three-dimensional landscape process modelling: the effect of DEM resolution. *Earth Surface Processes and Landforms* **25**(9): 1025–1034.

Takken I, Beuselinck L, Nachtergaele J, Govers G, Poesen J, Degraer G. 1999. Spatial evaluation of a physically-based distributed erosion model (LISEM). *CATENA* **37**(3–4): 431–447.

Takken I, Govers G, Jetten V, Nachtergaele J, Steegen A, Poesen J. 2005. The influence of both process descriptions and runoff patterns on predictions from a spatially distributed soil erosion model. *Earth Surface Processes and Landforms* **30**(2): 213–229.

Toutin T. 2002. Three-dimensional topographic mapping with ASTER stereo data in rugged topography. *IEEE Transactions on Geoscience and Remote Sensing* **40**(10): 2241–2247.

Van Oost K, Govers G, Desmet PJJ. 2000. Evaluating the effects of changes in landscape structure on soil erosion by water and tillage. *Landscape Ecology* **15**: 577–589.

Van Rompaey A, Govers G, Baudet M. 1999. A strategy for controlling error of distributed environmental models by aggregation. *International Journal of Geographical Information Science* **13**(6): 577–590.

Van Rompaey A, Govers G. 2002. Data quality and model complexity for regional scale soil erosion prediction. *International Journal of Geographical Information Science* **16**(7): 663–680.

Van Rompaey A, Bazzoffi P, Jones RJA, Montanarella L. 2005. Modeling sediment yields in Italian catchments. *Geomorphology* **65**(1–2): 157–169.

Van Rompaey AJJ, Verstraeten G, Van Oost K, Govers G, Poesen J. 2001. Modelling mean annual sediment yield using a distributed approach. *Earth Surface Processes and Landforms* **26**(11): 1221–1236.

Van Rompaey AJJ, Krasa J, Dostal T, Govers G. 2003. Modelling sediment supply to rivers and reservoirs in Eastern Europe during and after the collectivisation period. *Hydrobiologia* **494**: 169–176.

Van Zyl JJ. 2001. The Shuttle Radar Topography Mission (SRTM): a breakthrough in remote sensing of topography. *Acta Astronautica* **48**(5–12): 559–565.

Verstraeten G. 2006. Regional scale modelling of hillslope sediment delivery with SRTM elevation data. *Geomorphology* **81**(1–2): 128–140.

Verstraeten G, Van Oost K, Van Rompaey A, Poesen J, Govers G. 2002. Evaluating an integrated approach to catchment management to reduce soil loss and sediment pollution through modelling. *Soil Use and Management* **19**: 386–394.

Verstraeten G, Prosser IP, Fogarty P. 2007. Predicting the spatial patterns of hillslope sediment delivery to river channels in the Murrumbidgee catchment, Australia. *Journal of Hydrology* **334**(3–4): 440–454.

Vigiak O, Sterk G, Romanowicz RJ, Beven KJ. 2006. A semi-empirical model to assess uncertainty of spatial patterns of erosion. *CATEN*A **66**(3): 198–210.

Zhang X, Drake NA, Wainwright J, Mulligan M. 1999. Comparison of slope estimates from low resolution DEMs: scaling issues and a fractal method for their solution. *Earth Surface Processes and Landforms* **24**: 763–779.

DOI: 10.1002/esp